A Multilayer Structure Including a Ring Resonator for Measuring Permittivity of Lossy Materials

Gholamreza Moradi
Electrical Engineering Department, Amirkabir University of Technology, Tehran, Iran.
Email: Ghmoradi@aut.ac.ir

ABSTRACT:
This paper develops a permittivity measurement method using a multilayer microstrip structure. It provides modeling and analysis of the proposed structure. The employed method introduces new blocks in the multilayer microstrip model, which can cause more accurate characterization results. These blocks are for modeling the effect of different layers of the transmission line including the material under test and the other layers. Here, a multilayer planar measurement kit is provided for extracting the dielectric parameters of different materials. This measurement kit can measure relative permittivity as well as loss tangent for dielectrics. In addition, this kit can be used for characterization of solid and liquid dielectrics. The measurement setup is typically designed and fabricated for 2 GHz frequency, although it can cover higher frequencies *e.g.* X bands. The dominant mode and the higher order modes of the resonator can be used for measuring the material's parameters in a wide range of frequency. The analytic, simulation and measurement results illustrate good agreement with each other, which confirms the accuracy of the proposed routine.

KEYWORDS: Analytical models, Dielectric measurement, Material properties, Microwave measurements, Measurement techniques, Permittivity, Resonators, Q factor.

1. INTRODUCTION

Nowadays many different techniques are introduced for measuring electromagnetic parameters of materials. Most of the resonator-based measurement approaches employ waveguides [1-8], cavities [9-12], dielectrics [13-16] and transmission lines [17-21]. Another interesting technique for measuring dielectric properties is using ring resonator structures. The ring resonator is a ring shaped transmission line having several wavelengths length to avoid mutual inductance effects. The first microstrip ring resonator application was proposed by Troughton [22] for determination of phase velocity and dispersive characteristics of a microstrip line. For multi-layer structures, in 1968, [23, 24] developed a closed-form formula based on a variational calculation of the line capacitance in the Fourier-transformed domain to compute the effective permittivity of the multi-layer microstrip-like ring resonator and hence the resonant frequencies for several test materials. In 1992, Svacina proposed a new procedure for calculating effective complex permittivity and characteristic impedance based on conformal mapping [25, 26]. Analysis of microstrip ring resonator in multi-layer structures was reported in [27] with metal sheets in top and bottom.

A suspended ring resonator for dielectric constant measurement of foams is discussed and measured in [28, 29], that inspired by them, in this paper, a structure is proposed for a wide range of materials under test. In addition, accurate multi-layer analysis of this structure is described. The proposed structure is divided into a few parts and each part is modeled by its network matrix. Then, each section is analyzed to present the complete model of the whole structure. As a case study, the proposed structure is fabricated in S band, whose measurement results validate the analysis results very well.

2. STRUCTURE MODEL

The top view of the building blocks of the employed structure which is based on a ring resonator is shown in Fig. 1. A detailed version of side and top views of the proposed structure is shown in Fig. 2. This structure consists of two feed lines, which are located on the top of the lowest layer. The ground plane is in the bottom of the lowest layer. The feed lines are separated from the ring with two gaps (labeled with Δ) in two sides of the ring. The feed line and ring widths are respectively shown by W_f and W_r. In this structure, the sample matter covers the feed lines and the ring. L_f is the length of feed lines which is covered by sample and other layers. The radius of internal and external

تاریخ دریافت: ۱۳۹۹/۰۳/۲۳ تاریخ پذیرش: ۱۳۹۹/۰۵/۰۷

circles of the ring are respectively shown by R_1 and R_2. h_1, h_2 and h_3 are thickness, ϵ_1, ϵ_2 and ϵ_3 are relative permittivity and δ_1, δ_2 and δ_3 are loss tangent of the layers from bottom to top, respectively.

In this structure, as shown in Fig. 2 (a), the ring is located at a different level than the feed lines, and the sample exists as a separator between the ring and feed lines. So, the coupled field path is closed through the sample material. As a result, it is considerably affected by the sample material.

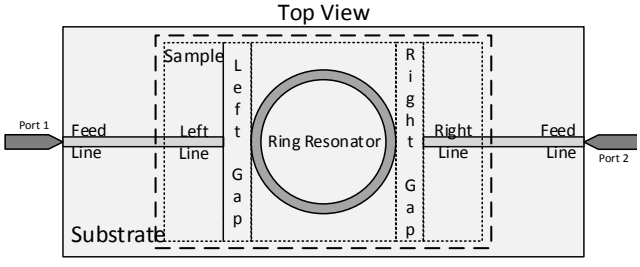

Fig. 1. Multilayer microstrip measurement kit based on ring resonator and its blocks.

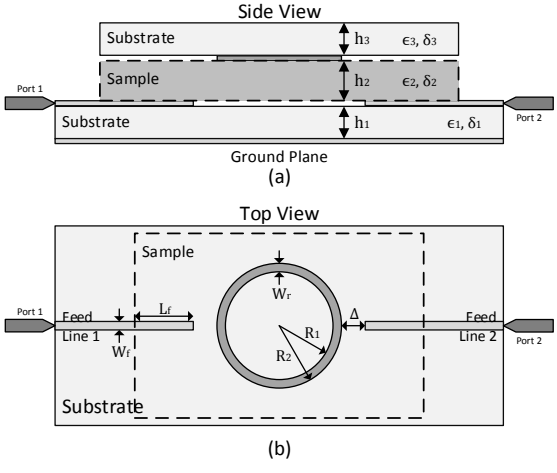

Fig. 2. Parameters of the proposed structure (a) Side view of the structure (b) Top view of the structure.

3. THEORY AND ANALYSIS

For a multilayer structure, [25] gives the complex effective permittivity of layers and [26] presents characteristic impedance of the transmission lines. The complex relative permittivity of each layer is well known as:

$$\epsilon_{r\,c_i} = \epsilon_{r\,i}(1 - j\tan\delta_i) \tag{1}$$

where $i = 1,2,\dots,N$ which are the indexes of layers. ϵ_{r_i} is relative permittivity of the i^{th} layer and $\tan\delta_i$ is loss tangent of the i^{th} layer. It is noticeable that we can express the complex permittivity versus its real and imaginary parts, or equivalently express it versus the real part and the loss tangent. Here the latter approach is followed.

Reference [25] defines effective permittivity of a multilayer structure based on conformal mapping method. The ratio of W to h is defined as a parameter of calculation of complex effective relative permittivity, where W is the width of transmission line and h is the height of the feed line from the ground plane. It is assumed that there are M layers bellow the transmission line and N layers above it. For $W \geq h$, the effective width of the transmission line is defined as:

$$W_e = W + \frac{2h}{\pi}\ln\left[17.08\left(\frac{W}{2h} + 0.92\right)\right] \tag{2}$$

$$q_i = \frac{H_i}{2}\left(1 + \frac{\pi}{4} - \frac{h}{W_e}\ln\left[\frac{2W_e\sin\left(\frac{\pi}{2}H_i\right)}{hH_i} + \cos\left(\frac{\pi H_i}{2}\right)\right]\right) - q_{i-1} \tag{3}$$

where $i = 1,2,\dots,M-1$ are indexes of layers bellow the transmission line. q_i is a parameter which is used in the continuation of the paper. H_i is defined as the ratio of height of upper support of the i^{th} layer from the ground plane to height of transmission line from the ground plane (4).

$$H_i = \frac{1}{h}\sum_{k=1}^{i} h_k \tag{4}$$

where $h_1, h_2, \dots, h_j$ are the height of substrate $1,2,\dots,j$ respectively.

For the M^{th} layer, the q_M is calculated as (5).

$$q_M = 1 - \frac{h}{2W_e}\ln\left[\frac{\pi W_e}{h} - 1\right] - q_{M-1} \tag{5}$$

For layers above the transmission line we have:

$$q_j = \frac{h}{2W_e}\left\{\ln\left[\frac{\pi W_e}{h} - 1\right] - \left(1 + V_j\right)\ln\left[2W_e\frac{\cos\left(\frac{\pi V_j}{2}\right)}{h\left(2H_j - 1 + V_j\right)} + \sin\left(\frac{\pi V_j}{2}\right)\right]\right\} \tag{6}$$

where $j = M+1,\dots,N-1$ and V_j is given by (7).

$$V_j = \frac{2h}{\pi}\tan^{-1}\left(\frac{\pi}{\frac{\pi W_e}{2h} - 2}(H_j - 1)\right). \tag{7}$$

q_N is obtained by (8) where N is the index of the upper layer of the stack.

$$q_N = 1 - \sum_{i=1}^{M} q_i - \sum_{j=M+1}^{N-1} q_j \tag{8}$$

The corresponding equations for $W < h$ are:

$$q_i = \frac{\ln A_i}{2\ln\left[\frac{8h}{W}\right]}\left(1+\frac{\pi}{4}-\frac{1}{2}\cos^{-1}\left[\frac{W\sqrt{A_i}}{8hH_i}\right]\right) \tag{9}$$

$$A_i = \frac{1+H_i}{1-H_i+\frac{W}{4h}}$$

$$q_M = 0.55 + \frac{0.9}{\pi \ln\left(\frac{8h}{W}\right)} - q_{M-1} \tag{10}$$

$$q_j = \frac{1}{2} - \frac{0.9+\frac{\pi}{4}\ln\left(B_j\right)\cos^{-1}\left(\left(1-\frac{1-\frac{W}{8h}}{H_j}\right)\sqrt{B_j}\right)}{\pi \ln\left(\frac{8h}{W}\right)} \tag{11}$$

$$B_j = \frac{1+H_j}{H_j+\frac{W}{4h}-1}$$

Finally the effective relative permittivity of multi-layer stack is:

$$\epsilon_{r_e} = \frac{(\sum_{i=1}^{M} q_i)^2}{\sum_{i=1}^{M} \frac{q_i}{\epsilon_{r_i}}} + \frac{(\sum_{j=M+1}^{N} q_j)^2}{\sum_{j=M+1}^{N} \frac{q_j}{\epsilon_{r_j}}} \tag{12}$$

Characteristic impedance is given by [26]:

$$W \geq h \Rightarrow Z_0 = \frac{120\pi h}{W\sqrt{\epsilon_{r_e}}} \tag{13}$$

$$W < h \Rightarrow Z_0 = \frac{60}{\sqrt{\epsilon_{r_e}}}\ln\frac{8h}{W}$$

The propagation constant i.e. γ of the transmission line is calculated by:

$$\gamma = j\omega\sqrt{\mu_0\epsilon_0\epsilon_{r_e}} \tag{14}$$

For analyzing the proposed measurement kit, volume under the sample is divided into 5 parts i.e.:

1. Length of the left transmission line which is covered by the sample material
2. The left gap between transmission line and the ring
3. The ring resonator
4. The right gap
5. Length of the right transmission line

The feed lines are 50 Ω microstrip transmission lines. In continuation of the paper, each of these parts are modeled by ABCD or transmission matrix parameters.

3.1. Left and Right Feed Lines

On the left and right feed lines of the structure where feed lines are under the sample, the characteristic impedance of feed lines changes. The characteristic impedance is calculated by (1) to (13), where $W = W_f$, which is the feed line width, and h is the height of the bottom layer. The characteristic impedance of feed lines is shown by Z_{0_f}. Since ϵ_{r_e} (in distance L_f) is complex, the transmission line is lossy. Considering this loss, the ABCD matrix is given by [28]:

$$\begin{bmatrix} A & B \\ C & D \end{bmatrix}_{\text{Left/Right Lines}} = \begin{bmatrix} \cosh(\gamma_f L_f) & Z_{0_f}\sinh(\gamma_f L_f) \\ \frac{1}{Z_{0_f}}\sinh(\gamma_f L_f) & \cosh(\gamma_f L_f) \end{bmatrix} \tag{15}$$

3.2. Left and Right Gaps

The feed line and ring resonator have a capacitive coupling with each other [29]. Therefore, the left and right gaps can be modeled as shown in Fig. 3.

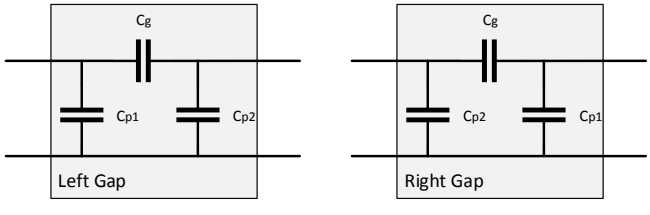

Fig. 3. Network models of the left and right gap.

The ABCD matrix of the left gap is easily calculated as:

$$\begin{bmatrix} A & B \\ C & D \end{bmatrix}_{\text{Left Gap}} = \begin{bmatrix} 1+\frac{C_{P_2}}{C_g} & \frac{1}{j\omega C_g} \\ j\omega\left(C_{P_1}+C_{P_2}+\frac{C_{P_1}\times C_{P_2}}{C_g}\right) & 1+\frac{C_{P_1}}{C_g} \end{bmatrix} \tag{16}$$

and similarly that of the right gap is:

$$\begin{bmatrix} A & B \\ C & D \end{bmatrix}_{\text{Right Gap}} = \begin{bmatrix} 1+\frac{C_{P_1}}{C_g} & \frac{1}{j\omega C_g} \\ j\omega\left(C_{P_1}+C_{P_2}+\frac{C_{P_1}\times C_{P_2}}{C_g}\right) & 1+\frac{C_{P_2}}{C_g} \end{bmatrix} \tag{17}$$

In these equations, calculation of the capacitors necessitates having ϵ_{r_e} which is the effective complex permittivity of the feed line in multilayer structure, which by itself is calculated from (1) to (12). The typical values of the elements for our case study are $C_{p1} = 1360\ fF$, $C_{p1} = 1360\ fF$ and $C_g = 850\ fF$. It is noticeable that, the ring resonator and feed lines are in different levels so the parallel capacitor must be divided into two capacitors [29] as shown in Fig. 4.

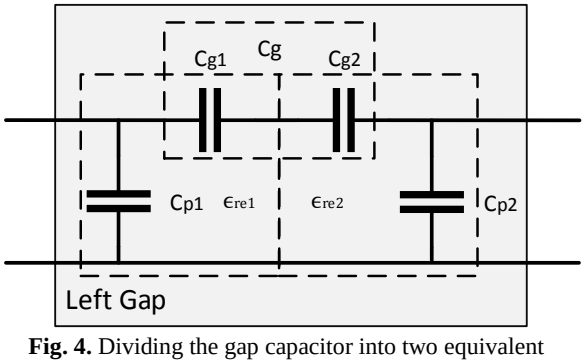

Fig. 4. Dividing the gap capacitor into two equivalent capacitors in the network model of the gap.

The left gap model used for this structure is shown in Fig. 4. For this structure, C_{p_1} and C_{g_1} are calculated using effective permittivity of the feed line ($\epsilon_{r_{e1}}$) and C_{p_2} and C_{g_2} are calculated using effective permittivity of the ring resonator ($\epsilon_{r_{e2}}$). At last, the C_g is obtained by series combination of C_{g_1} and C_{g_2} as given in (18).

$$C_g = \frac{C_{g_1} C_{g_2}}{C_{g_1} + C_{g_2}} \tag{18}$$

For the right gap, the mirror of the model in Fig. 4 must be used.

3.3. Ring Resonator

In two-port network analysis of the ring resonator, we consider it as two parallel transmission lines. Therefore, using the ABCD matrix in (15), the Y matrix is given by:

$$\begin{bmatrix} Y_{11} & Y_{12} \\ Y_{13} & Y_{14} \end{bmatrix} = \begin{bmatrix} \frac{1}{Z_{0_r}}\left[\coth(\gamma_r l_1) + \coth(\gamma_r l_2)\right] & \frac{-1}{Z_{0_r}}\left[\operatorname{csch}(\gamma_r l_1) + \operatorname{csch}(\gamma_r l_2)\right] \\ \frac{-1}{Z_{0_r}}\left[\operatorname{csch}(\gamma_r l_1) + \operatorname{csch}(\gamma_r l_2)\right] & \frac{1}{Z_{0_r}}\left[\coth(\gamma_r l_1) + \coth(\gamma_r l_2)\right] \end{bmatrix} \tag{19}$$

where Z_{0_r} is characteristic impedance of the ring and $l_1 = l_2 = \pi R_{av}$ is the half circumference of average circle in the ring. In other words, R_{av} is radius of average circle, *i.e.* $R_{av} = (R_1 + R_2)/2$. Z_{0_r} and γ_r are calculated from (1) to (13). It is noticeable that $W = W_r$ is the width of ring and $h = H_1 + H_2$ is the height of bottom layer plus that of the sample. Considering $l_1 = l_2$, (19) can be reduced to:

$$\begin{bmatrix} Y_{11} & Y_{12} \\ Y_{21} & Y_{22} \end{bmatrix} = \begin{bmatrix} \frac{2\left(e^{\gamma_r l} + e^{-\gamma_r l}\right)}{Z_{0_r}\left(e^{\gamma_r l} - e^{-\gamma_r l}\right)} & \frac{-4}{Z_{0_r}\left(e^{\gamma_r l} - e^{-\gamma_r l}\right)} \\ -\frac{-4}{Z_{0_r}\left(e^{\gamma_r l} - e^{-\gamma_r l}\right)} & \frac{2\left(e^{\gamma_r l} + e^{-\gamma_r l}\right)}{Z_{0_r}\left(e^{\gamma_r l} - e^{-\gamma_r l}\right)} \end{bmatrix} \tag{20}$$

where $l = l_1 = l_2$. Finally, by converting Y matrix to ABCD [30], the ABCD matrix is obtained as:

$$\begin{bmatrix} A & B \\ C & D \end{bmatrix}_{\text{Ring}} = \begin{bmatrix} \frac{\left(e^{\gamma_r l} + e^{-\gamma_r l}\right)}{2} & \frac{Z_{0_r}\left(e^{\gamma_r l} - e^{-\gamma_r l}\right)}{4} \\ \frac{\left(e^{\gamma_r l} - e^{-\gamma_r l}\right)}{Z_{0_r}} & \frac{\left(e^{\gamma_r l} + e^{-\gamma_r l}\right)}{2} \end{bmatrix} \tag{21}$$

3.4. Device Model

According to the obtained matrices, whole ABCD matrix of the device is given by:

$$\begin{bmatrix} A & B \\ C & D \end{bmatrix}_{\text{Device}} = \begin{bmatrix} A & B \\ C & D \end{bmatrix}_{\text{Left Line}} \begin{bmatrix} A & B \\ C & D \end{bmatrix}_{\text{Left Gap}} \begin{bmatrix} A & B \\ C & D \end{bmatrix}_{\text{Ring}} \begin{bmatrix} A & B \\ C & D \end{bmatrix}_{\text{Right Gap}} \begin{bmatrix} A & B \\ C & D \end{bmatrix}_{\text{Right Line}} \tag{22}$$

from which, S_{21} is calculated by:

$$S_{21} = \frac{2}{A + \frac{B}{Z_0} + CZ_0 + D} \tag{23}$$

3.5. Model parameters

For the proposed structure, the geometrical and physical parameters are shown as Table I.

It should be mentioned that the feed lines and ring resonator are implemented on FR4 substrates, which is a very cheap and available PCB.

4. MEASUREMENT AND RESULTS

Here, the analytic results are compared with the simulation and measurement results. The simulation is done with CST Microwave Studio software. It is well

known that variation in relative permittivity can cause frequency shifting in return loss response of the structure. Comparison of simulation and analytic results of permittivity has been done for $\tan\delta = 0.01$, and is shown in Fig. 6, which shows very good agreement between the simulation and analytic results.

The ϵ' of MUT can be extracted from measurement of the frequency shift. Similarly, ϵ'' or loss tangent is measured from bandwidth or the amplitude decreasing rate of S_{21}.as will be discussed in the continuation of the paper.

Increase of loss tangent decreases the amount of amplitude in a given resonant frequency. The decreasing rate of amplitude of simulation and analytic results (for $\epsilon_r = 1.5$) is compared in Fig. 7. As seen, the two decreasing rates are the same.

The influence of loss tangent on S_{21} parameter is presented in Fig. 8. The loss tangent is extracted from (24) where f_0 is the resonant frequency and BW_0 is bandwidth around the resonant frequency.

$$\tan\delta = \frac{f_0}{BW_0} \tag{24}$$

This structure is fabricated and measured as shown in Fig. 9. In this measurement, the MUT is a composite with $h_2 = 1.1mm$, $\epsilon_r = 1.3$ and $\tan\delta = 0.015$. Fig. 10 depicts the measurement, simulation and analytical results of transmission parameter, i.e. S_{21}, of the overall structure. A good agreement between analytic and measurement results are observed. Similarly, Table 2 shows that the permittivity of the three methods match well with each other.

Symbol	Quantity	Description
L_f	7.96 mm	Transmission Line covered with MUT1
W_f	1.55 mm	Width of the Feed Line
W_r	1.55 mm	Width of the Ring Resonator
R_1	15.062 mm	Inner Radius of the Ring Resonator
R_2	15.5526 mm	Outer Radius of the Ring Resonator
Δ	0.2 mm	The Gap Between Feed Line and Ring
h_1	0.8 mm	Thickness of the Lower Layer
ϵ_1	4.3	Relative Permittivity of the Lower Layer
δ_1	0.025	Tangent Delta of the Lower Layer
h_3	0.8 mm	Thickness of the Upper Layer
ϵ_3	4.3	Relative Permittivity of the Upper Layer
δ_3	0.025	Tangent Delta of the Upper Layer

Table 1. Parameters of the proposed Structure.

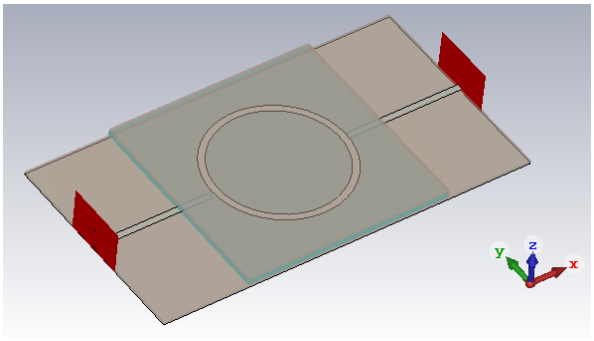

Fig. 5. Implementation of the Structure in CST Microwave Studio.

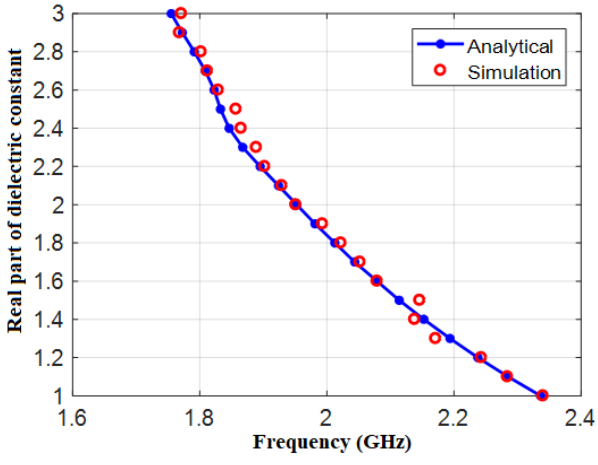

Fig. 6. Resonant frequency variation with variation of ϵ_r.

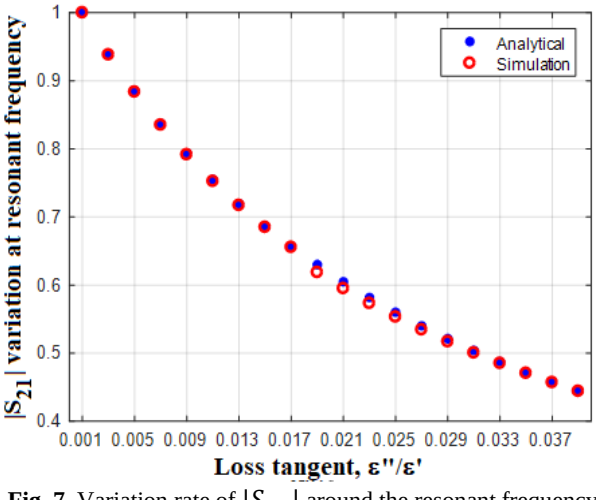

Fig. 7. Variation rate of $|S_{21}|$ around the resonant frequency versus variation of loss tangent.

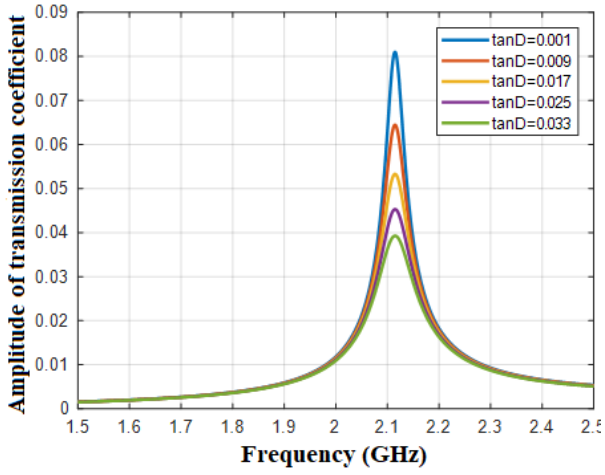

(a) Analytical data

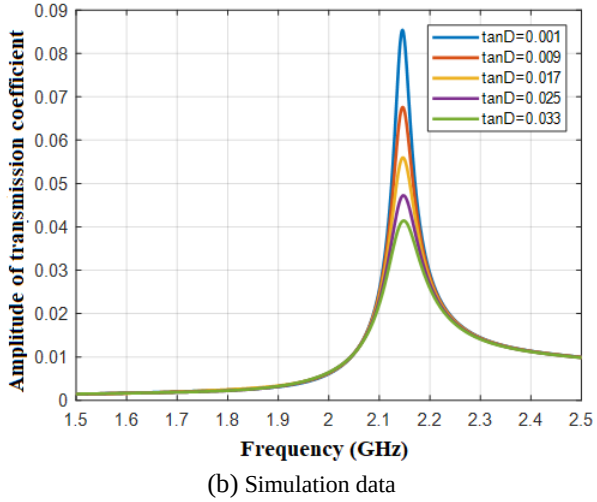

(b) Simulation data

Fig. 8. Amplitude variation rate at the resonant frequency for some loss tangents.

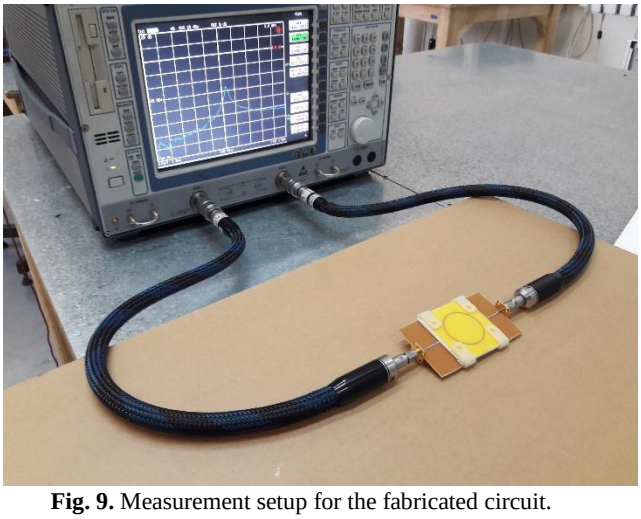

Fig. 9. Measurement setup for the fabricated circuit.

5. CONCLUSION

Designing a general purpose, simple, cheap and accurate measurement setup with minimum physical limitation has been discussed. This goal was achieved by a multilayer ring resonator structure. The MUT was sandwiched between two substrates. A ring resonator including two gaps was used for measuring the parameters of the dielectric under test. The results show that a very good agreement exists between measurement, CST Microwave Studio simulation and analytic results. The proposed routine can be used for characterization of both solid and liquid materials.

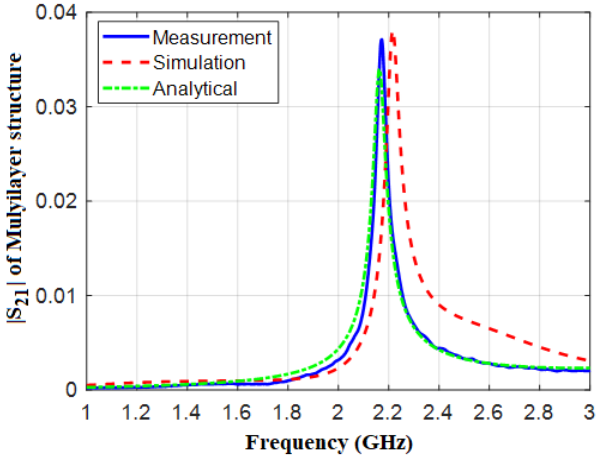

Fig. 10. Comparison of measurement, simulation and analytic results of S_{21}.

	ϵ_r	$\tan\delta$
Real Values	1.3	0.015
Simulation	1.34	0.016
Analytic	1.28	0.013

Table 2. Measurement, Simulation and Analytical Values of permittivity.

REFERENCES

[1] M. M. Scott, D. L. Faircloth, J. A. Bean, and S. G. Holliday, "Biaxial permittivity determination for electrically small material specimens of complex shape using shorted rectangular waveguide measurements," IEEE Trans. Instrum. Meas., vol. 63, no. 4, pp. 896-903, 2014.

[2] V. N. Skresanov, Z. E. Eremenko, E. S. Kuznetsova, Y. Wu, and Y. He, "Circular layered waveguide use for wideband complex permittivity measurement of lossy liquids," IEEE Trans. Instrum. Meas., vol. 63, no. 3, pp. 694-701, 2014.

[3] F. Fesharaki, C. Akyel, and K. Wu, "Broadband permittivity measurement of dielectric materials using discontinuity in substrate integrated waveguide," Elect. Lett., vol. 49, no. 3, pp. 194-196, 2013.

[4] M. J. Akhtar and M. Thumm, "Measurement of complex permittivity of cylindrical objects in the E-plane of a rectangular waveguide," IEEE Trans Geosci Remote Sens, vol. 51, no. 1, pp. 122-131, 2013.

[5] F. Costa, C. Amabile, A. Monorchio, and E. Prati, "Waveguide dielectric permittivity measurement technique based on resonant FSS filters," IEEE Microw. Wirel. Compon. Lett, vol. 21, no. 5, pp. 273-

275, 2011.
[6] E. Kilic, A. Yapar, and F. Akleman, “Complex permittivity determination of dielectric materials by waveguide measurements: A robust approach based on integral equations,” IEEE Microw. Wirel. Compon. Lett, vol. 21, no. 11, pp. 631-633, 2011.
[7] U. Hasar, C. Westgate, and M. Ertugrul, “Permittivity determination of liquid materials using waveguide measurements for industrial applications,” IET Microw Antenna P., vol. 4, no. 1, pp. 141-152, 2010.
[8] U. C. Hasar, “Accurate complex permittivity inversion from measurements of a sample partially filling a waveguide aperture,” IEEE Trans. Microw. Theory Tech, vol. 58, no. 2, pp. 451-457, 2010.
[9] A. Kik, “Complex permittivity measurement using a ridged waveguide cavity and the perturbation method,” IEEE Trans. Microw. Theory Tech, vol. 64, no. 11, pp. 3878-3886, 2016.
[10] A. H. Sklavounos and N. S. Barker, “Liquid-permittivity measurements using a rigorously modeled overmoded cavity resonator,” IEEE Trans. Microw. Theory Tech, vol. 62, no. 6, pp. 1363-1372, 2014.
[11] C. Rosenberg, N. Hermiz, and R. Cook, “Cavity resonator measurements of the complex permittivity of low-loss liquids,” IEE Proc H Microwaves Optic Antenn, vol. 129, no. 2, pp. 71-76, 1982.
[12] M. Olyphant, “Microwave permittivity measurements using disk cavity specimens,” IEEE Trans. Instrum. Meas., vol. 1001, no. 4, pp. 342-344, 1971.
[13] T. Shimizu, H. Inada, and Y. Kogami, “Complex permittivity measurement for a low loss dielectric rod using a novel 50 GHz band TM 010 mode cavity,” IEEE Microwave Measurement Conference (ARFTG), 89th ARFTG, pp. 1-4, 2017.
[14] A. Nakayama and H. Yoshikawa, “Permittivity measurements at millimeter wave frequencies using dielectric rod resonator excited by NRD-guide,” J. Eur. Ceram. Soc, vol. 26, no. 10-11, pp. 1853-1856, 2006.
[15] A. Nakayama, A. Fukuura, and M. Nishimura, “Millimeter-wave measurement of complex permittivity using dielectric rod resonator excited by NRD-guide,” IEEE Trans. Microw. Theory Tech, vol. 51, no. 1, pp. 170-177, 2003.
[16] G. Annino, M. Cassettari, M. Martinelli, and P. Van Bentum, “A nonradiative approach to single-mode dielectric resonators,” Appl. Magn. Reson., vol. 24, no. 2, p. 157, 2003.
[17] U. C. Hasar, “Determination of Complex Permittivity of Low-Loss Samples From Position-Invariant Transmission and Shorted-Reflection Measurements,” IEEE Trans. Microw. Theory Tech, 2017.
[18] J. Naqui et al., “Transmission lines loaded with pairs of stepped impedance resonators: modeling and application to differential permittivity measurements,” IEEE Trans. Microw. Theory Tech, vol. 64, no. 11, pp. 3864-3877, 2016.
[19] P. M. Narayanan, “Microstrip transmission line method for broadband permittivity measurement of dielectric substrates IEEE Trans. Microw. Theory Tech, vol. 62, no. 11, pp. 2784-2790, 2014.
[20] D. Zhao, G. Rietveld, and G. M. Teunisse, “A multistep approach for accurate permittivity measurements of liquids using a transmission line method,” IEEE Trans. Instrum. Meas., vol. 60, no. 7, pp. 2267-2274, 2011.
[21] U. C. Hasar, “Unique retrieval of complex permittivity of low-loss dielectric materials from transmission-only measurements,” IEEE Geos. Remote Sens. Lett., vol. 8, no. 3, pp. 562-564, 2011.
[22] P. Troughton, “Measurement techniques in microstrip,” Elect. Lett., vol. 2, no. 5, pp. 25-26, 1969.
[23] E. Yamashita, “Variational method for the analysis of microstrip-like transmission lines,” IEEE Trans. Microw. Theory Tech, 16, no. 8, pp. 529-535, 1968.
[24] E. Yamashita and R. Mittra, “Variational method for the analysis of microstrip lines,” IEEE Trans. Microw. Theory Tech, vol. 16, no. 4, pp. 251-256, 1968.
[25] J. Svacina, “A simple quasi-static determination of basic parameters of multilayer microstrip and coplanar waveguide,” IEEE Microw. Wirel. Compon. Lett, vol. 2, no. 10, pp. 385-387, 1992.
[26] J. Svacina, “Analysis of multilayer microstrip lines by a conformal mapping method,” IEEE Trans. Microw. Theory Tech, vol. 40, no. 4, pp. 769-772, 1992.
[27] P. Bernard and J. Gautray, “Measurement of dielectric constant using a microstrip ring resonator,” IEEE Trans. Microw. Theory Tech, vol. 39, no. 3, pp. 592-595, 1991.
[28] S. Waldron and S. Makarov, “Measurement of dielectric permittivity and loss tangent for bulk foam samples with suspended ring resonator method,” 2006 IEEE Antennas and Propagation Society International Symposium, Albuquerque, NM, 2006, pp. 3175-3178, doi: 10.1109/APS.2006.1711285.
[29] S. Waldron, S. Makarov, S. Biederman and R. Ludwig, “Suspended Ring Resonator for Dielectric Constant Measurement of Foams,” in IEEE Microwave and Wireless Components Letters, vol. 16, no. 9, pp. 496-498, Sept. 2006, doi: 10.1109/LMWC.2006. 880708.